Linking fragmentation with the evolutionary stage: grain growth and astrochemistry in the Infrared Dark Cloud G14.225-0.506

Author: Anna Hill Romero
Facultat de Física, Universitat de Barcelona, Diagonal 645, 08028 Barcelona, Spain.

Advisor: Gemma Busquet Rico

Abstract: We present Submillimeter Array observations of the 1 mm dust continuum emission and a molecular line survey towards hub-S of the Infrared Dark Cloud G14.225-0.506. We aim to probe grain growth and chemical composition of the dense cores to determine their evolutionary stage. We detected 7 cores and estimated their dust emissivity index using the Rayleigh Jeans approximation and assuming optically thin emission, finding values from 0 to 1.5, lower than the typical value of the interstellar medium ($\sim$1.6), indicating the presence of large grains (millimeter-sized). We underline the presence of deuterated species and interstellar complex organic molecules, mainly methanol, in some cores. All cores exhibit carbon monoxide and other simple molecules. The results suggest that cores MM1a, MM3a and MM5b are in an advanced evolutionary stage within the protostellar phase, whereas MM4, MM5a and MM7a may be less evolved young stellar objects.

I. INTRODUCTION

The fragmentation of a molecular cloud, which ends up in the formation of stellar clusters, is a process that depends on multiple physical parameters of the dense cores, such as the temperature, the density structure, the level of turbulence, the intensity and orientation of the magnetic field and the amount of angular momentum. Additional effects, like the evolutionary stage and/or different environmental conditions may also play an important role in the fragmentation process. The way to evaluate these two possible scenarios is to analyze separately the dust emissivity index of the dust grains and the chemical composition of the dense cores.

Dense cores are gravitationally bound condensations of gas and dust associated with protostar formation. The dust emissivity index, β, and its variations can be related to the dust grain properties such as size, porosity and surface composition [1]. The typical emissivity index for the diffuse interstellar medium is ~ 1.6 [2], indicating μm-sized dust grains, while internal envelopes of deeply embedded protostars could manifest $\beta \sim 1$ [3, 4], suggesting the growth of dust grains in Young Stellar Objects (YSOs).

The chemistry of dense cores presents a strong dependence on the physical conditions (mainly density and temperature) during the star formation process [5]. In cold and dense cores, with temperatures of ~ 10 K and densities of $10^4 - 10^6$ cm^{-3}, molecules in the gas phase freeze and stick to the surface of dust grains [6]. This results in the enhancement of deuterated species and the hydrogenation of CO atoms, the second most abundant molecule after H_2. In a more evolved stage within the protostellar phase, with densities above 10^7 cm^{-3}, the heating of the infalling envelope to hundreds of Kelvin allows the mobility of molecules that are likely to form interstellar complex organic molecules (iCOMs) [6].

In the southwest of the HII region M17, we find the Infrared Dark Cloud G14.225-0.506 (hereafter IRDC G14.2). Located at a distance of 1.6 kpc [7], it consists of a network of dense filaments forming two hub-filament systems [8]. Observations carried out with the Submillimeter Array (SMA) at 1.3 mm with an angular resolution of $\sim$ 1.5" showed that the two hubs present a different level of fragmentation, being hub-S more fragmented than hub-N. Nevertheless, all the derived physical properties and their values are remarkably similar in both hubs [9]. Thus, temperature and density profiles, the level of turbulence, the rotational-to-gravity energy and the surrounding magnetic field cannot explain the differences in the degree of fragmentation.

In this work, we will focus on the study of hub-S, the southern hub of IRDC G14.2. We will carry out an analysis of the dust emissivity index, β, to probe grain growth. Independently, we will examine the chemical composition of the dense cores by conducting a molecular line survey, since the presence or absence of some key species can be related to the evolutionary stage of the cores.

II. OBSERVATIONS AND DATA PROCESSING

The data analyzed in this work was obtained with the SMA ([10]; proposal code 2021A-S054). The SMA is a radio interferometer located in Maunakea (Hawaii) with 8 antennas of 6 m dishes operating at submm/mm wavelengths. The observations were conducted with the compact configuration on 2021 June 21, covering a total bandwidth of $\sim$48 GHz (from 208 GHz to 220 GHz, from 228 GHz to 251 GHz and from 258 GHz to 271 GHz).

The image reconstruction from the visibility data was performed using the *tclean* task of the Common Astronomy Software Applications (CASA [11]). This procedure was used to generate, separately, continuum images and spectral line cubes. The *tclean* task is based on the CLEAN algorithm proposed by Högbgom (1974) [12]. The task implements the inverse Fourier transform of the visibilities in order to get the sky brightness distribution known as the "dirty" image. Through an iterative process, the function finds the brightest pixel of a region, subtracts a fraction of its flux, and substitutes its magnitude in the model image until it reaches a threshold. The task also enables us to assign different weights to each visibility by varying the "robust" parameter. The coefficient values range from -2, where we get higher resolution but

a reduction of the sensitivity, to +2, where sensitivity is maximum but the PSF widens. Both continuum and line images were computed using a robustness equal to 0.

We generated a continuum image of each frequency interval of the three detailed before and a single image using the total bandwidth. Additionally, we produced 24 spectral line cubes with a bandwidth of ~ 2.3 GHz each. The threshold value was set at 3.6 mJy for continuum images and 4.5 mJy for spectral cubes. The synthesized beam of the continuum and spectral cubes are 3.0" $\times$ 2.6" and 3.4" $\times$ 3.2", respectively, and the root-mean-square (rms) noise level is 1.3 mJy/beam for the continuum and 60 mJy/beam per spectral channel.

III. RESULTS AND DISCUSSION

A. Dust continuum emission

In Figure 1 (top panel), we present the dust continuum emission at 1 mm generated with the maximum bandwidth coverage ($\sim$48 GHz). We can observe the fragmentation of hub-S into different dense cores. The condensations have been labeled according to [9]. We detected 7 cores with emission above 6σ and with closed contour levels, being σ the rms noise level. In these regions, identified with white circles, we will later estimate the observed spectral index and perform molecular line identification.

The bottom panel of Figure 1 shows the spectral index map. The spectral index is defined as

$$\alpha = \frac{\log\left(S_{\nu_1}/S_{\nu_0}\right)}{\log\left(\nu_1/\nu_0\right)}, \tag{1}$$

being S_ν the flux density and ν the frequency. In the Rayleigh Jeans approximation and assuming optically thin emission at millimeter wavelengths, spectral index values translate to a dust emissivity index $\beta = \alpha - 2$.

The spectral index map was produced using the *immath* task of CASA in *spix* mode, which computes the spectral index from two continuum images of different frequencies. We selected ν_1 and ν_0 as the upper and lowermost frequency side bands, with center frequencies at 265 and 214 GHz, respectively. We estimated α as the mean of pixel values enclosed within the circular regions indicated in the top panel of Figure 1. We considered the uncertainty of the measure as the combination of the standard deviation and the $\sim$10% uncertainty in flux calibration. The results and the corresponding values of β are included in Table *I*.

The observed range of values for the emissivity index is consistent with those detected during the protostellar phase. We found that MM1a, MM3a and MM5b exhibit emissivities close to zero, suggesting important grain growth and more evolved dense cores. This behavior contrasts with the relatively high $\beta \sim 1.5$ derived in MM5a, similar to the dust emissivity index of 1.6 found in the interstellar medium, with μm-sized dust grains. This indicates that MM5a could correspond to a protostellar core in a very early evolutionary stage, since its value matches the ones found in the inner envelopes of deeply embedded YSOs [4]. Finally, we notice that MM4 and MM7a have intermediate dust emissivity indices, $\beta \sim 0.7$ and $\beta \sim 0.6$ respectively, but low enough values to expect considerable large grains. Thus, they will be at a more advanced evolutionary stage than MM5a.

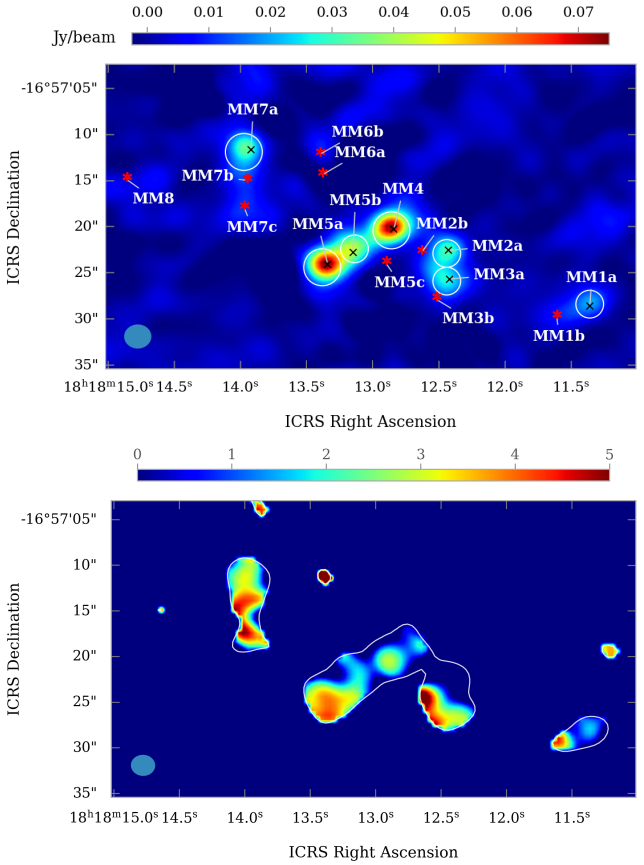

FIG. 1: *Top:* Map of the SMA dust continuum emission of G14.2 hub-S. Black crosses correspond to the positions of the cores with high enough emission to be detected; red stars depict the positions of other faint sources identified in [9]. The white circular contours surround the regions with emission greater than 6σ. *Bottom:* spectral index map performed with $\nu_1 = 264$ GHz and $\nu_0 = 214$ GHz (see Eq. 1), with 6σ contour level of the continuum image in white. The synthesized beams are shown in the bottom left corner.

The maximum size of the dust grain population is proportional to the observed wavelength. When it is significantly smaller than the observed wavelength, the value of β tends to be high, similar to the one found in the interstellar medium. When the maximum size is larger than the observed wavelength, low values of β are expected. Hence, the presence of $\beta < 1$ in most of the cores suggests that the dust grains have reached millimeter sizes, as observations were carried out at 1 mm.

In our study, we considered that all flux comes from dust thermal emission. However, in protostellar envelopes, we may have contamination from either thermal free-free and/or synchrotron emission. Although the contribution at millimeter

TABLE I: Flux density, spectral index and dust emissivity index of the identified dense cores.

Source ID	$S_{214\text{GHz}}$ (mJy) [a, b]	$S_{239\text{GHz}}$ (mJy) [a, b]	$S_{264\text{GHz}}$ (mJy) [a, b]	$\alpha_{214-264\text{GHz}}$	$\beta_{214-264\text{GHz}}$
MM1a	11.2 ± 1.1	14.2 ± 1.4	20 ± 2	1.4 ± 1.0	$\sim 0 \pm 1.0$
MM2a	16.4 ± 1.6	21 ± 2	20 ± 2	–	– [c]
MM3a	11.4 ± 1.1	21 ± 2	26 ± 3	2.2 ± 1.0	0.2 ± 1.0
MM4	44 ± 4	67 ± 7	95 ± 10	2.7 ± 1.0	0.7 ± 1.0
MM5a	44 ± 4	144 ± 14	123 ± 12	3.5 ± 1.1	1.5 ± 1.1
MM5b	18.1 ± 1.8	28 ± 3	38 ± 4	2.0 ± 1.0	$\sim 0 \pm 1.0$
MM7a	23 ± 2	37 ± 4	68 ± 7	2.6 ± 1.1	0.6 ± 1.1

Notes
[a] 214, 239 and 264 GHz are the center frequencies of each band side.
[b] The flux calibration uncertainty is estimated to be ~ 10 %.
[c] Source is not resolved in the spectral index map.

wavelengths is usually negligible and systematically below $\sim 10\%$, it can differ depending on the core and could lead to a deviation of the results. Furthermore, another potential source of error could be that the central regions of the cores are optically thick. To verify whether the hypothesis of optically thin emission is reasonable, it would be necessary to study the relationship between the flux density, S_ν, and the Planck function at dust temperature, $B_\nu(T)$, and ensure the profiles fulfill: $S_\nu/\Omega = B_\nu(T)$ (see [3]). In addition, in order to obtain a more reliable estimation of β we should consider that envelopes are affected by central luminosity and the temperature of the sources depends on the radius.

B. Molecular line identification

In this section, we present a chemical study of G14.2 hub-S. Using data from the entire ∼48 GHz bandwidth covered by the SMA, we generated 24 spectral line cubes of ∼2.3 GHz bandwidth each. From every individual image, we extracted the spectrum of the 7 detected sources in the dust continuum image (white circles highlighted in the top panel of Figure 1). Therefore, we obtained 7 different spectra from a single image, resulting in a total of 168 spectra. The extraction process was carried out using CASA. We corrected the shift in frequencies due to the source velocity of $\sim$ 20 km s^{-1} [8]. The identification of molecular lines was conducted by comparing our spectra with spectral line surveys performed in similar regions and within the same frequency ranges as those analyzed in this work [13–17]. Moreover, we consulted the *Splatalogue* database for astronomical spectroscopy [18] to verify the identification of lines and determine their transition and upper energy level. We extracted a total of 124 lines from the spectra and identified 31 molecular transitions corresponding to 19 different species, some of which appear in more than one core. However, we were unable to identify the transition of certain lines as they were consistent with multiple molecules. Observations at higher spectral resolution are needed to avoid line blending problems.

In order to illustrate the identification process, in Figure 2 we display two spectral cubes extracted from MM4 and MM3a, representing the rest frequency ranges of 217.7–220.0 GHz and 260.7–263.0 GHz, and labeling the identified molecular lines. MM4 is as an example of a chemically rich core, in contrast to MM3a, where we were only able to identify one line within this range. Furthermore, we observe that its intensity is significantly lower compared to the same line detected in MM4. It is clear that, in order to surely distinguish a line from the noise signal, it needs to be relatively above the baseline level.

In Table II, we classify into four categories all the distinct molecular species identified: 1) deuterated, containing deuterium; 2) outflows, tracing the mass ejection in protostellar envelopes; 3) simple molecules, with less than 6 atoms; 4) iCOMs, interstellar complex organic molecules with 6 or more atoms. The entire number of transitions of each type, per core, is documented in Figure 3.

TABLE II: Molecular species detected.

Deuteraded	DCO^+, DCN
Outflows	CO, $C^{18}O$
Simple molecules	C_2H, H_2CO, HCO^+, $H^{13}CO^+$, HCN, $H^{13}CN$, HC_3N, $C^{34}S$, CS, ^{34}SO, SO
iCOMs	CH_3OH, CH_3OOH, CH_3CN, CH_3CHNH

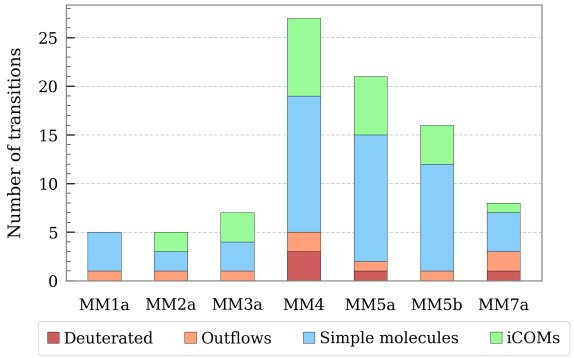

FIG. 3: Number of identified transitions in each core, classified according to Table II.

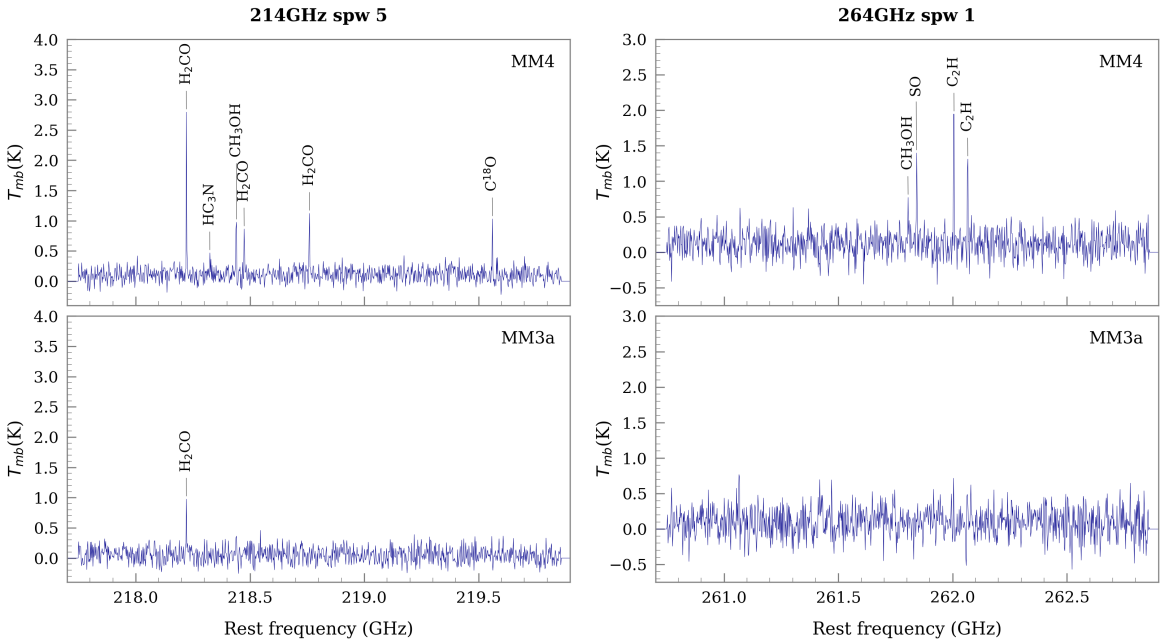

FIG. 2: Spectral line cubes for MM4 (top) and MM3a (bottom). We show spectral window 5 of $208 - 220$ GHz side band (left spectra) and spectral window 1 of $258 - 271$ GHz band (right spectra). The image includes the molecular lines identified.

We emphasize the low number of identified transitions in MM1a, MM2a, MM3a. The outflow tracer detected in them is carbon monoxide (CO), the second most abundant molecule in cold molecular clouds after H_2, and the main molecular gas tracer through the study of its rotational transitions. The line is associated with the transition $J = 2 \rightarrow 1$ at 230.539 GHz with upper energy $E_{\rm u} = 16.596$ K. Additionally, in all of them stands out the presence of the hyperfine transitions $3_{(1,3)} \rightarrow 2_{(1,2)}$ and $3_{(0,3)} \rightarrow 2_{(0,2)}$ of H_2CO at 211.211 GHz and 218.325 GHz, respectively. H_2CO is typically found in the envelopes of YSOs, resulting from the hydrogenation of CO. The main difference lies in the fact that MM2a and MM3a exhibit iCOMs, unlike MM1a. One of the distinctive iCOMs identified is methanol (CH_3OH), formed from interactions of CO with the molecular hydrogen in the cloud or in the dust grains and then realized back to the gas when the temperature is high enough, upward of 100 K [5].

In contrast, we can highlight the chemical richness of MM4 and MM5a, with 27 and 21 transitions detected, respectively. Among the simple molecules, in addition to H_2CO, we can underline the presence of HCO^+ and HCN, along with their isotopotologues $H^{13}CO^+$ and $H^{13}CN$, with energies around $E_u \approx 25$ K. An enhancement of these species could be found in cold environments where another important process takes place: the deuterium fractionation. Deuterium, noticed in both cores, commonly appears in young and not excessively hot regions. Regarding iCOMs, we primarily detect methanol transitions over a wide range of frequencies, from ∼218 GHz to ∼267 GHz. We mainly identify the transitions between $J = 5 \rightarrow 4$ levels with energies ranging from $E_{\rm u} \approx 16 - 57$ K. The dissociation of methanol produces radicals that, when reacting with other spices, result in the production of iCOMs with a larger number of atoms, like acetic acid (CH_3COOH), recognized in MM5b.

For a more exhaustive study of molecular lines and the derivation of their physical properties, it could be appropriated to use a lower value of the robust parameter to gain resolution in the line images and be able to determine the position of peaks more accurately, or even distinguish different peaks within the same line, which are not resolved.

C. Grain growth and chemical composition

The aim of this section is trying to link the results of the dust emissivity indices and the molecular content in each core with its evolutionary stage.

First, we can analyze MM1a, MM3a, and MM5b. All three cores have $\beta \sim 0$ and we did not detect deuterated species in their spectra. The main difference between them is the presence or lack of complex molecules. We do not identify iCOMs in MM1a, which leads to two hypotheses about its evolutionary state. On the one hand, it could be a low-mass protostar with a low temperature, preventing the evaporation of iCOMs from the icy dust mantles. On the other hand, it could be a notably evolved core, thus with larger dust grains, that has already lost part of its envelope and has accreted most of the gas. This possibility would be consistent with the presence of CO, which would trace molecular outflows that spread the envelope out, and with the low number of transitions observed. MM3a and MM5b do exhibit iCOMs. Even so, we can expect them to be rather evolved objects for two reasons: the low value of their emissivity index and the absence of deuterated molecules, that appear in early

protostellar phases. However, we can infer that they are slightly less evolved objects compared to MM1a or that they exhibit a higher temperature in order to release iCOMs frozen in dust grains. Although we have not been able to determine the spectral index of MM2a, based on the chemical content, we can expect it to be in a similar stage to MM3a and MM5b.

Separately, we can study MM4, MM5a, and MM7a. In these cores, besides iCOMs, we are able to identify spectral lines corresponding to deuterated molecules, which indicates they are young protostellar cores. This remark is in agreement with their higher emissivity indices. Nevertheless, we cannot find an explanation for why MM4 and MM7a have $\beta \sim 0.7$ while for MM5a we found $\beta \sim 1.5$. Distinguishing the chemical composition of MM5a from the other two cores based on the identified spectral lines, it is neither simple nor evident, so it would be necessary to analyze other factors. Observations at longer wavelengths, 3 mm for instance, would help in differentiating the evolutionary stage of these cores.

IV. CONCLUSIONS

In this work, we present the results obtained from 1 mm observations carried out with SMA towards hub-S of the IRDC G14.2. We estimated the dust emissivity index of the resolved cores in the continuum map to probe grain growth in the envelopes of YSOs. In addition, we performed a molecular line identification in the spectra extracted from each core. Our study leads to the following conclusions:

1. The dust emissivity index of the detected cores ranges between 0 and 1.5, suggesting that grain growth already occurs in the envelopes of young protostars.
2. Regarding the chemical composition, we underline the presence of deuterated molecules and the detection of iCOMs, mainly methanol, in some cores. The outflow tracer CO has been identified in all cores.
3. MM1a exhibits β close to zero. The non-detection of deuterium and iCOMs suggests that it may be in an advanced evolutionary stage and has already lost part of its envelope.
4. MM3a and MM5b show values of $\beta \sim 0$, too. We did not detect deuterated species, but iCOMs are present. Thus, they could be relatively less evolved or have a higher temperature compared to MM1a.
5. MM4a, MM5a and MM7 manifest similar chemical composition, having deuterated species and iCOMs, as well as high values of the β. This implies they could be very young objects. However, the reason why the emissivity index of MM4 and MM7 is lower than that of MM5a cannot be explained through the analysis of the chemical composition.

Further analysis of the emissivity index correcting for potential contaminating emission (free-free and/or non-thermal), optically thick emission and the presence of an internal luminosity and observations at longer wavelengths with higher angular and spectral resolution are needed to find additional differences in the evolutionary stage of the cores.

Acknowledgments

I would like to express my sincere gratitude to Dra. Gemma Busquet for her invaluable guidance, constant support and encouragement. I also want to thank my family and friends for being by my side throughout this emotional roller-coaster.

[1] N. Ysard et al. (2019), "From grains to pebbles: the influence of size distribution and chemical composition on dust emission properties". *A&A*, **631**, A88.
[2] Plank collaboration. (2014), "Planck 2013 results. XI. All-sky model of thermal dust emission". *A&A*, **571**, A11.
[3] M. Galametz et al. (2019), "Low dust emissivities and radial variations in the envelopes of Class 0 protostars: possible signature of early grain growth". *A&A*, **632**, A5.
[4] J. K. Jørgensen et al. (2017), "A Submillimeter Array Survey of Low-Mass Protostars. I. Overview of Program: Envelopes, Disks, Outflows, and Hot Cores". *ApJ*, **659**, 478.
[5] J. K. Jørgensen, et al. (2020), "Astrochemistry during the formation of stars". *A&A, Annual Review*, **58**, 727.
[6] P. Caselli and C. Ceccarelli. (2012), "Our astrochemical heritage". *A&ARv*, **20**, 56.
[7] C. Zucker et al. (2020), "A compendium of distances to molecular clouds in the Star Formation Handbook". *A&A*, **633**, A51.
[8] G. Busquet et al. (2013), "Unveiling a Network of Parallel Filaments in the Infrared Dark Cloud G14.225-0.506". *ApJ Letter*, **764**, L26.
[9] G. Busquet et al. (2016), "What is controlling the fragmentation in the Infrared Dark Cloud G14.225–0.506?: Different levels of fragmentation in twin hubs". *ApJ*, **819**(2), 139.
[10] "Submillimeter Array Observer Centre (SMA)". `http://sma1.sma.hawaii.edu`
[11] "Common Astronomy Software Applications (CASA)". `https://casa.nrao.edu/`
[12] J. Högbom (1974), "Aperture synthesis with a non-regular distribution of interferometer baselines". *A&A, Suppl. Ser.*, **15**, 417.
[13] A. Belloche et al. (2013), "Complex organic molecules in the interstellar medium: IRAM 30 m line survey of Sagittarius B2(N) and (M)". *A&A*, **559**, A47.
[14] G.A. Blake, E.C. Sutton, C.R. Masson and T.G. Phillips. (1986), "The rotational emission-line spectrum of Orion A between 247 and 263 GHz". *ApJ, Suppl. Ser.*, **60**, 357.
[15] J.S. Greaves and G.J. White (1991), "A 257-273 GHz spectral survey of the OMC1 cloud core". *A&A, Suppl. Ser.*, **91**, 237.
[16] A. Nummelin, P. Bergman, A. Hjalmarson et al. (1998), "A three-position spectral line survey of sagitarius B2 between 218 and 263 GHz". *ApJ, Suppl. Ser.*, **117**, 427.
[17] E.C. Sutton et al. (1986), "Molecular line survey of Orion from 215 to 247 GHz". *ApJ, Suppl. Ser.*, **58**, 341.
[18] "Splatalogue. Database for astronomical spectroscopy". `https://splatalogue.online/`